physica **p·s·s** status solidi **c**

current topics in solid state physics

Ground State of Electron-Hole Bilayer
Kazuo Yamashita, Kenichi Asano,
Takuma Ohashi

physica **p·s·s** status solidi **b**

www.pss-b.com

basic solid state physics

New article series

Advanced Calculations
for Defects in Materials –
Electronic Structure
Methods

Feature Article

Chris G. Van de Walle
and Anderson Janotti

physica **p·s·s** status solidi **a**

www.pss-a.com

applications and materials science

Expert Opinion
Solid-state lighting
Roland Haitz and Jeffrey Y. Tsao

WILEY-VCH

physica **p·s·s** status solidi **rrl**

www.pss-rapid.com

rapid research letters

New: review@rrl

Competing energy scales in
high-temperature superconductors:
Ultrafast pump-probe studies
Elbert E. M. Chia, Jian-Xin Zhu,
D. Talbayev, and A. J. Taylor

WILEY-VCH

WILEY-VCH

physica **pss** status solidi **a**
www.pss-a.com
applications and materials science

Tailored design of boron-doped diamond electrodes for various electrochemical applications with boron-doping level and sp²-bonded carbon impurities

Takeshi Watanabe[1], Yuki Honda[1], Kazuhiro Kanda[2], and Yasuaki Einaga*,[1,3]

[1] Department of Chemistry, Keio University, 3-14-1 Hiyoshi, Yokohama 223-8522, Japan
[2] Laboratory of Advanced Science and Technology for Industry, University of Hyogo, 3-1-2 Koto, Kamigori, Ako-gun, Hyogo 678-1205, Japan
[3] CREST, Japan Science and Technology Agency, 5 Sanbancho, Chiyoda, Tokyo 102-0075, Japan

* Corresponding author: e-mail einaga@chem.keio.ac.jp, Phone: +81 45 566 1704, Fax: +81 45 566 1697

The effects of sp²-bonded carbon impurities on the electrochemical properties of boron-doped diamond were investigated in moderately ($[B] < 10^{20}$ cm^{-3}) and heavily ($[B] > 10^{21}$ cm^{-3}) boron doping levels. Significant influences of sp²-bonded carbon impurities, which show glassy carbon-like electrochemical properties after anodic oxidation, were observed in heavily boron-doped diamond. This indicated that the significant effects of enhanced adsorption properties were possibly caused by surface relaxation of the strains induced by heavy boron doping and sp²-bonded carbon impurities. On the other hand, their durability was still similar to diamond electrodes rather than glassy-carbon electrodes because of the low fraction of sp²-bonded carbon impurities. Such "active" diamond electrodes are much less suitable for wastewater treatment than ordinary diamond electrodes due to a different oxygen-evolution mechanism. On the other hand, "active" BDD electrodes have a much higher efficiency for electrochemical ozone production than other BDD electrodes. The electrode properties of BDD can be designed by controlling the boron doping level and introducing the sp²-bonded carbon impurities. The guidelines proposed in this study can be used effectively to design electrodes according to their individual application, such as for use as electrochemical sensors, in wastewater treatment or electrochemical ozone production.

1 Introduction Much attention has been drawn to conducting boron-doped diamond (BDD) as an electrode material for electrochemical sensors because of its superior electrochemical properties, such as the low background current and wide potential window [1–3]. Moreover, the intrinsic durability of diamond is highly advantageous for electrolytic applications [4]. It is known that BDD electrodes show high resistance to electrochemical corrosion, whereas sp²-bonded carbon materials such as glassy carbon are brittle when used as highly polarized anodes [5–7]. In addition, they are effective for wastewater treatment, since BDD electrodes can efficiently generate hydroxyl (OH) radicals that are highly oxidative species due to the large over-potential for the oxygen-evolution reaction (OER) [8]. These electrochemical properties of BDD electrodes have been applied for the electrochemical production of ozonized water [9].

Thus, although diamond is a candidate electrode material for various electrochemical applications, each application does not necessarily require the same properties. Consequently, the electrode design appropriate for each application is important in order to bring out the full potential of diamond. Although the inert properties of diamond electrodes are thought of as advantages, "active" diamond electrodes can also be utilized as versatile electrodes if it is possible to control the properties.

The electrochemical properties of diamond can be substantially affected by the boron doping concentration [10, 11], surface termination [11, 12] and nondiamond sp^2-bonded carbon impurities [13, 14]. In particular, because the boron concentration determines the electrical conductivity of diamond, it can strongly influence the electrochemical properties. It is known that BDD changes from an insulator to a metal with increasing boron doping and the critical point has been reported by Bustarret et al. [15] as being $4–5 \times 10^{20}$ atoms cm^{-3}.

The surfaces of electrodes are always important for electrochemistry, hence in the case of diamond surface-terminated atoms can affect the electrochemical response. Furthermore, it is known that hydrogenated undoped diamond exhibits surface conductivity due to surface transfer doping [16, 17].

Nondiamond sp^2-bonded carbon impurities also affect the electronic structure, and their effect is more complicated. The electrochemical behavior of sp^2-bonded carbon material is more highly active compared to diamond, while they are much less durable than diamond [18].

Composite materials of sp^2–sp^3-bonded carbon are commonly called amorphous carbon or diamond-like carbon (DLC) according to the fraction of sp^2 and sp^3. The electrical conductivity of such materials varies depending on the ratio or the concentrations of hydrogen and dopant. DLC (sp^3-rich composite) normally behaves inherently as an insulator unless the DLC includes specific dopants [19]. Although the boundaries between sp^2-bonded carbon, amorphous carbon, DLC, and diamond are not clearly defined and somewhat confusing, in this paper, the films, which mainly have a diamond structure, are considered to be diamond despite a small amount of sp^2-bonded carbon impurity.

The effects of sp^2-bonded carbon impurities have seldom been studied while those of boron doping and surface termination have been reported much more. Swain and coworkers [13] studied the effects of sp^2-bonded non-diamond carbon impurities on BDD electrodes and reported that the impurities play an important role in the electrode reaction kinetics for certain redox systems. However, the effects of sp^2-bonded carbon impurities combined with boron doping level have hardly been investigated. It is expected that the effect of sp^2-bonded carbon impurities may also be affected by the boron doping level. On the other hand, the addition of sp^2-bonded carbon impurities to diamond causes deformation of the rigid sp^3-bonded carbon network structure. Therefore, a constructive approach advancing a material by incorporating sp^2-bonded carbon is uncommon in electrochemistry of diamond.

In this work, we investigate the effect of sp^2-bonded carbon impurities on the electrochemical properties in different boron doping levels. The two groups for boron doping level were prepared based on the critical point of metal–insulator transition ($4–5 \times 10^{20}$ atoms cm^{-3}). Moderately BDD films were prepared to be lower than 10^{20} atoms cm^{-3} and heavily boron-doped films were prepared to be higher than 10^{21} atoms cm^{-3}. An sp^2-bonded carbon impuri-

ties-contained BDD film was prepared for each boron doping level. The amounts of sp^2-bonded carbon impurities in the films were controlled to be low enough to retain the durability of diamond. These four different types of BDD in boron doping level and sp^2-bonded carbon content were fabricated and their electrochemical properties and their capabilities for the each application were investigated.

2 Experimental Four types of polycrystalline BDD thin films were grown on Si (111) substrates using a 2.45 GHz microwave plasma chemical vapor deposition (CVD) system equipped with a 6 kW microwave plasma CVD reactor (CORNES Technologies Corp., Model AX6500). The details of the diamond growth are presented in the Supporting Information (online at: www.pss-a.com).

The boron concentrations in the diamond were estimated by secondary ion mass spectroscopy (SIMS) using an IMS-7f (CAMECA). The surface morphology and the film thickness were examined with a field emission scanning electron microscope (FE-SEM) using SIRION (FEI). The resistivity of the films was measured by the van der Pauw method utilizing a Sourcemeter 2400 and Nanovoltmeter 2182A (Keithley) after removing Si substrate with an acid mixture of HF and HNO$_3$. Raman spectra were recorded in ambient air at room temperature with an Acton SP2500 (Princeton Instruments) under excitation at 532 nm from a green laser diode.

Cyclic voltammetry was conducted with a potentiostat (HZ-5000, Hokuto Denko Corp.) using a single-compartment three-electrode PTFE cell with an Ag/AgCl (saturated KCl) reference electrode and a Pt coiled wire counterelectrode. The electrical contacts for electrochemical measurements were made by connecting copper wires to the BDD surface with silver paste. The CV measurements were performed at the hydrogenated surface and oxygenated surfaces. Hydrogenated surfaces were prepared by exposure to hydrogen plasma after washing it in aqua regia. Oxygenated surfaces were prepared by potential cycling between 0–4 V vs. Ag/AgCl for 10 cycles in 0.1 M sulfuric acid. Hydrogenated and oxygenated surfaces were checked by contact-angle measurement with water drops. The flow-injection analysis (FIA) with electrochemical detection (FIA-ECD) system consisted of a microliquid chromatography pump (PU712i, GL Science), an injector with a 20 μl injection loop (9725i, GL Science), an amperometric detector with a thin layer flow cell (ED703pulse, GL Science), and a data-acquisition system (EZ Chrome Elite, Scientific Software Inc.). A 1 mM formic acid was used as a test analyte in a 0.1 M PBS carrier solution with pH 6.8 at a regulated flow rate of 1 mL min^{-1}. The measurements of electrolytic ozone production were performed using a flow-type ozonated water generator (OPENICS-220, NIKKA MICRON CO., LTD.). The electrolytic flow cell used was a zero gap cell equipped with a Nafion$^{®}$ membrane sandwiched between the anode and cathode. The perforated BDD electrodes to be evaluated were used as anodes and another perforated BDD electrode was utilized as the cathode for the measurements. The electrolyte solution in deionized water had a flow rate of 1.08 L min^{-1} and

Phys. Status Solidi A 211, No. 12 (2014)

Original

Paper

2711

the ozone concentration was monitored with a diaphragm polarograph-type dissolved ozone meter (OZ-20, DKK-TOA Co., Japan) placed downstream from the anode. The voltage and current between the anode and cathode were recorded with a data logger (GL220, Graphtec Co., Japan).
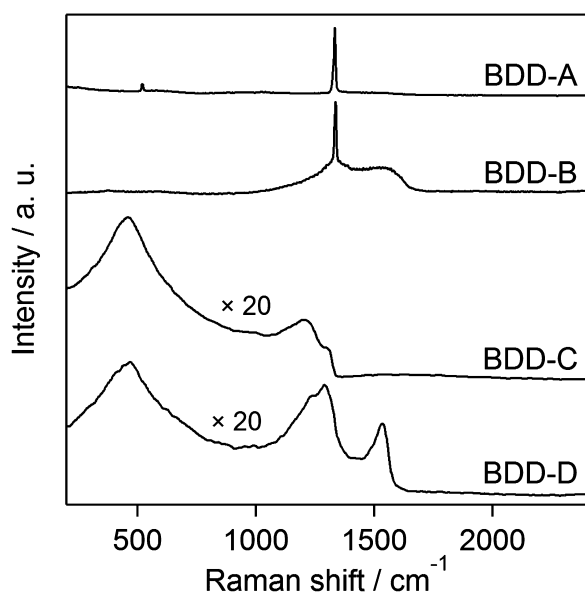
3 Results and discussion

3.1 Structural characterization The boron concentrations [B], in the four prepared BDD films were estimated by SIMS. The boron concentrations, the resistivity at room temperature and the thickness of the synthetic BDD films are summarized in Table 1. Here, these four electrodes are designated as BDD-A, BDD-B, BDD-C, and BDD-D. These electrodes can be divided into moderately doped films (BDD-A, and -B) and heavily doped films (BDD-C and -D) based on the critical point of metal–insulator transition (4–5×10^{20} atoms cm^{-3}) [15]. The carbon network structures of these BDD films were investigated by Raman spectroscopy (Fig. 1). In the spectra of the BDD-A and BDD-B, the sharp peak of the center zone optical phonon of diamond can clearly be observed at 1332 cm^{-1}. In the spectrum of BDD-C, this peak has shifted to lower wave numbers and can be

Table 1 Boron concentration and resistivity of the synthetic films.

sample	B/C ratio of feed gas (ppm)	boron density by SIMS (atoms cm^{-3})	film thickness (μm)	resistivity at RT (Ω cm)
BDD-A	100	7.1×10^{19}	12	1.7
BDD-B	100	5.9×10^{19}	16	0.90
BDD-C	10,000	2.6×10^{21}	1.6	1.8×10^{-3}
BDD-D	50,000	5.5×10^{21}	3.2	3.3×10^{-3}

Figure 1 Raman spectra of synthetic BDD electrodes. Excitation wavelength is 532 nm.

observed on the shoulder of a band at around 1220 cm^{-1}. This shift, which is observed in heavily doped diamond, is due to quantum interference between this phonon and the continuum of electronic transitions (the so-called "Fano effect") [20, 21]. In the spectrum of BDD-D, the shifted peaks were broadened, suggesting the deformation of the diamond lattice. The large bands observed at around 470 and 1220 cm^{-1} in the spectra of the BDD-C and BDD-D are normally observed in metallic, heavily BDD. These bands are assigned to be related to maxima in the phonon density of states of diamond [22]. In the spectra of BDD-B and BDD-D, a peak, which can be attributed to the D band and G band of sp^2-bonded carbon, appears at around 1300 and 1500 cm^{-1}, respectively. Although the Raman spectra indicate that BDD-B and -D contain some nondiamond sp^2-bonded carbon impurities, the fraction of sp^2-bonded carbon is very low because the cross-sectional scattering coefficient for nondiamond sp^2-bonded carbon is ~50 times larger than that for diamond [23]. The X-ray diffraction patterns also confirm that all of the films have the structure of diamond (data not shown) and the X-ray absorption spectra also show the fraction of sp^2-bonded carbon is very low even in BDD-B and BDD-D (Fig. S1, see Supporting Information, online at: www.pss-a.com). According to the SIMS and Raman spectra, the four prepared BDD electrodes were confirmed as possessing different compositions in terms of their boron doping level and sp^2-bonded carbon content.

**3.2 Electrochemical properties** Figure 2 shows the background current-potential (i–E) curves, in 0.1 M HClO$_4$, scanned at a rate of 100 mV s^{-1}, for the prepared BDD electrodes before (a) and after (b) anodic treatment. The anodic treatment of the BDD films was performed by cycling potential from 0 V to +4.0 V for 10 cycles. The voltammograms were recorded between the anodic and cathodic potentials at which the current density reached ±250 μA cm^{-2}. The potential window, which is defined as this scanning region, tends to decrease with increasing boron doping level and the presence of sp^2-bonded carbon impurities. The BDD-A and BDD-B are regarded as p-type semiconductors according to the critical point of the metal–insulator transition. When a species in solution has energy levels in the bandgap of the semiconductor, p-type electrodes cannot carry out reduction due to downward band bending [24]. Although the standard potential for hydrogen-evolution reaction lies within the bandgap of diamond, cathodic current were observed at BDD-A and BDD-B. Latto et al. [11] have explained this behavior often observed at semiconducting BDD by a surface-state-mediated charge-transfer mechanism. In their experiment, hydrogen-terminated BDD showed semimetallic behavior even at boron doping densities lower than 10^{19} cm^{-3}, while oxygen-terminated BDD showed semiconducting behavior at the same boron doping density. In our results, moderately BDD with hydrogen termination showed similar behavior to metallic heavily BDD although the cathodic limits of potential windows are shifted to more negative potential. On the other hand, oxygen-terminated moderately BDD also showed
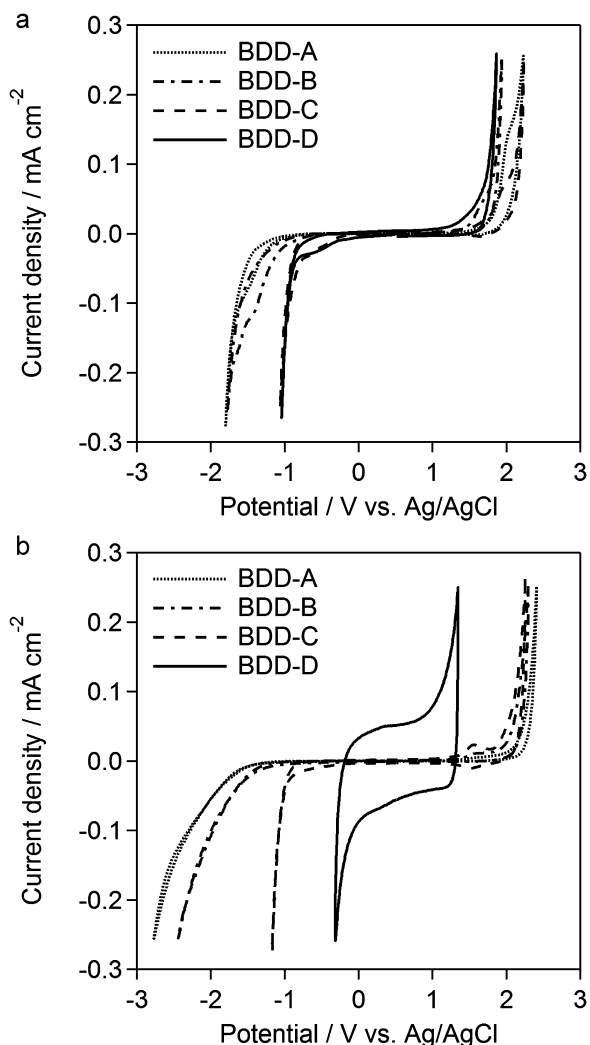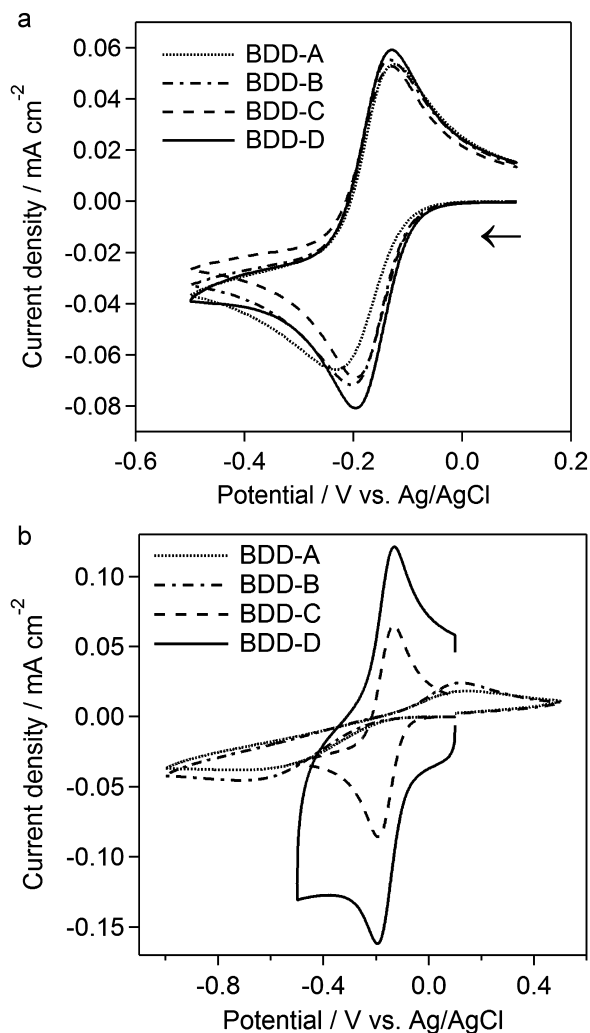
Figure 2 Background current–voltage curves of the synthetic BDD electrodes in 0.1 mol dm^{-3} HClO$_4$ solutions, (a) before and (b) after anodic treatment at a scan rate of 0.1 V s^{-1}.

In our previous work, heavily BDD electrodes including sp^2-bonded carbon impurities had a much higher background current than ordinary BDD electrodes in 0.5 M H$_2$SO$_4$ solutions [25]. The voltammograms of these electrodes resembled glassy carbon (GC) electrodes rather than ordinary BDD electrodes, despite the small fraction of sp^2-bonded carbon impurities. As in the previous work, the CV curve for the BDD-D electrode showed a GC-like behavior exhibiting a double-layer region and large charging current. Comparison of BDD-D with BDD-C suggests that the sp^2-bonded carbon impurities make a significant contribution to the electrochemical properties. However, there are no notable differences for moderately BDD in the presence or absence of sp^2-bonded carbon impurities.

The electrochemical properties were also investigated by cyclic voltammetry using [Ru(NH$_3$)$_6$]$^{2+/3+}$ as an inorganic complex and dopamine as electroactive organic compounds. Figure 3 shows the CV curves for [Ru(NH$_3$)$_6$]$^{2+/3+}$ with

Figure 3 Cyclic voltammograms of the synthetic BDD electrodes for 1 mmol dm^{-3} [Ru(NH$_3$)$_6$]Cl$_3$ in 1 mol dm^{-3} KCl solutions, (a) before and (b) after anodic treatment at a scan rate of 0.1 V s^{-1}.

hydrogen evolution current which should not be observed at p-type semiconducting diamond electrode, while the current was slightly inhibited. This indicates that the BDD-A and BDD-B electrodes are inhomogeneous and consist of semiconducting domains and semimetallic domains.

With respect to the heavily doped electrodes, the hydrogen-evolution current after anodic oxidation still steeply increased, unlike the moderately doped electrodes because the whole area of the electrodes are considered to be metallic in heavily doped electrodes. The voltammograms of BDD-C before and after anodic treatment are almost the same except for the small redox couples observed at the oxidized surface, which are attributed to electroactive surface functional group. On the other hand, the voltammogram of BDD-D was drastically changed by anodic treatment. The background current increased more than 100 times higher and potential windows became almost half that at the hydrogenated surface.

Phys. Status Solidi A 211, No. 12 (2014)

2713

BDD electrodes at a scan rate of $100\,\mathrm{mV\,s^{-1}}$ before and after anodic treatment. This is a typical redox analyte that proceeds through outer-shell electron transfer, and is commonly used for assessing electrode properties as well as ferri/ferrocyanide. A summary of the separations between potentials with oxidation and reduction peaks before and after anodic treatment is presented in Table 2.
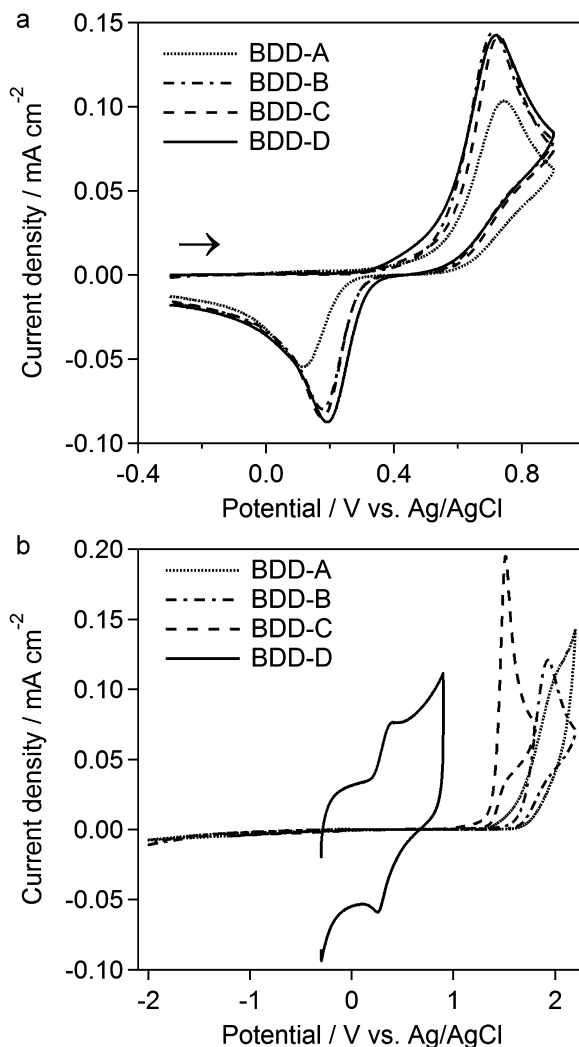
In the voltammograms recorded at hydrogenated surfaces (Fig. 3a), all BDD electrodes showed near-reversible behavior although BDD-A showed slightly larger peak potential separations. After anodic treatment, the peak potential separations for BDD-A and BDD-B were enlarged, while those of BDD-C and BDD-D retain the reversible behavior. Because the energy level for this redox also lies within the bandgap of diamond, these behaviors for the moderately BDD electrodes are associated to the inhomogeneities and surface-state-mediated charge-transfer mechanism. On the other hand, BDD-C and BDD-D contains many more boron atoms than the threshold for the insulator–metal transition, and their bulk metallic behavior is predominant compared to the changes at the surface. On the other hand, $\mathrm{sp^2}$-bonded carbon impurities have no large influences on the response for this redox system although the oxygenated BDD-D showed a high background current.

Figure 4 shows CV curves for dopamine at a scan rate of $100\,\mathrm{mV\,s^{-1}}$ before and after anodic oxidation. Dopamine is a neurotransmitter in the brain, and is an important target species in studies of the brain. Recently, the *in vivo* detection of dopamine has been attempted using BDD microelectrodes [26]. Dopamine is electroactive and its electrochemical reactions generally proceed through inner-sphere electron transfer [14, 27]. Therefore, the electron-transfer kinetics of dopamine are strongly dependent on the surface chemistry of the electrodes. Since it has been suggested that BDD electrodes can be used as suitable electrochemical sensors for biological species, it is important to determine the relationship between the properties of these electrodes and their response to the biological species.

In the voltammograms before anodic treatment, shown in Fig. 4a, oxidation and reduction peaks are observed for all BDD electrodes. Similar to the trend in Fig. 3, the positions of the peaks for the BDD-A are slightly different from those for the other BDD electrodes. In the voltammograms of BDD-A, BDD-B, and BDD-C after anodic treatment, the oxidation peaks were largely shifted to positive potential and reduction


Figure 4 Cyclic voltammograms of the synthetic BDD electrodes for $1\,\mathrm{mmol\,dm^{-3}}$ dopamine in $1\,\mathrm{mol\,dm^{-3}}$ KCl solutions, (a) before and (b) after anodic treatment at a scan rate of $0.1\,\mathrm{V\,s^{-1}}$.

peaks could no longer be observed. The results imply surface termination has more significant influences on response to dopamine than boron concentration because the difference in voltammograms between the oxygenated BDD-A and the oxygenated BDD-C is smaller than the changes by anodic treatment. It should be noted that BDD-D after anodic treatment showed an apparently different voltammgram from the other BDD including BDD-C which contains a similar concentration level of boron. The oxidation and reduction peaks were observed and the peak-potential separation was smaller than that before the anodic treatment. This difference between BDD-C and BDD-D indicates that the $\mathrm{sp^2}$-bonded carbon in BDD-D plays a catalytic role in dopamine oxidation and also acts as an adsorption site for the reactants. Actually, after the measurements the redox couple was also detected in a 1 M KCl solution without dopamine.

Table 2 Summary of peak potential separations in cyclic volatmmograms for 1 mM $[\mathrm{Ru(NH_3)_6}]\mathrm{Cl_3}$ before and after anodic treatments.

sample	H-terminated surface (V)	O-terminated surface (V)
BDD-A	0.108	0.876
BDD-B	0.070	0.842
BDD-C	0.066	0.060
BDD-D	0.067	0.063

On the other hand, the response with BDD-B after anodic oxidation was sluggish as well as BDD-A despite the inclusion of sp^2-bonded carbon impurities. It seems that a small amount of sp^2-bonded carbon impurities have no impact on the electrochemical properties of moderately BDD.

3.3 For wastewater treatment The suitability for wastewater treatment utilizing hydroxyl radicals was evaluated by measuring the oxidation of formic acid. Formic acid is very resistant to oxidation and generally less electrochemically active, and it does not give any clear oxidation peaks in the potential window. On the other hand, hydroxyl radicals that can be generated by applying a high potential to the BDD electrode are known as strong oxidants that oxidize and decompose organics almost indiscriminately [28]. Therefore, BDD can indirectly oxidize formic acid by electrochemically generating hydroxyl radicals. Formic acid is also utilized as a model substance for evaluating the capability for degradation of organics because simple oxidation reaction is given as

$$HCOOH + 2OH \rightarrow 2H_2O + CO_2. \tag{1}$$
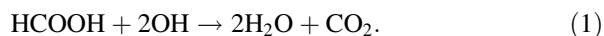
Comninellis proposed a comprehensive model for the anodic oxidation of organics [28]. The proposed scheme is summarized in the Supporting Information (Scheme S1).

When evaluating the ability of an electrode for the electrochemical mineralization of organics, it is difficult to extract only the current signal derived from oxidation of the organic compounds because the OER occurs at the same time. A FIA that is normally a fluid amperometric method and gives a signal when an injected sample passes by the electrode, can be a convenient approach for such a purpose [29].

Figure 5 shows the variation with potential of the signal current (a) and the background current (b). A 0.1 M phosphate buffer solution was used for the mobile phase at a flow rate of $1\,ml\,min^{-1}$ and $20\,\mu l$ of $1\,mmol\,dm^{-3}$ formic acid was injected three times at each potential. In the measurements, the background current represents the current derived from a series of OERs and the signal current represents the increment from the background current when an injected sample passes the electrode surface. Since direct electrochemical reactions of formic acid hardly ever occur, the direct cause for the signal current is regarded as mainly being oxidation of H_2O to hydroxyl radicals (reaction 2 in Supporting Information).

Because the amount of hydroxyl radicals at the electrode surface should be dependent on the electrode potential according to the Nernst equation, a consumption of the hydroxyl radicals by reactions with formic acid promotes the water oxidation to form hydroxyl radicals. Therefore, the magnitude of this signal current implies the ability to generate hydroxyl radicals that are consumed by reactions with organics. On the other hand, OER also consumes hydroxyl radicals and is therefore competitive reaction with mineralization reactions.

As seen in Fig. 5a, in BDD-A, B, and C signal current increased from about 2.0 V and the current maxima were
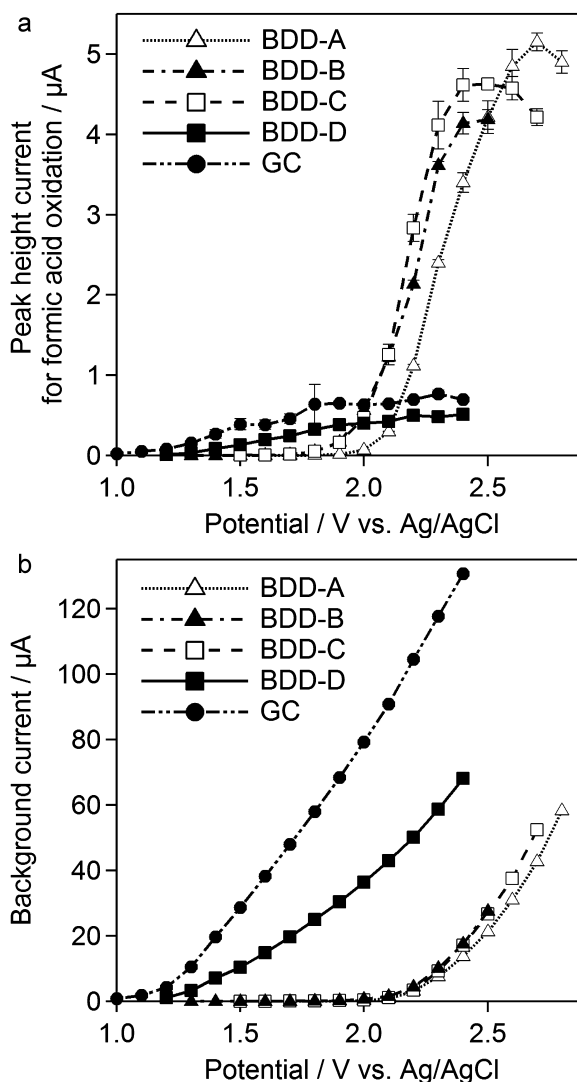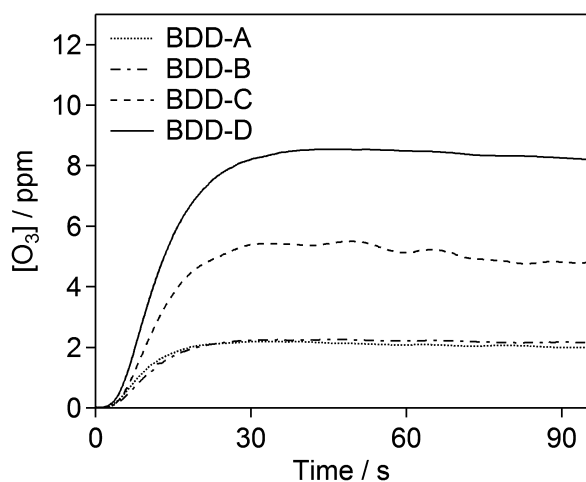

Figure 5 The variation with potential of (a) the FIA current signal with $1\,mmol\,dm^{-3}$ formic acid injection and (b) the background current for the synthetic BDD electrodes and a glassy carbon electrode. At more positive potential than displayed potentials, measurements were disturbed by bubble formation. In (a), the background currents were subtracted from the observed current.

obtained at 2.7 V for BDD-A and at 2.5 V for BDD-B and -C. For potentials around 2 V, the surface concentration of hydroxyl radicals is considered to be relatively low and hydroxyl radicals are consumed mainly by mineralization of formic acid (reaction 6 in SI), while at higher potentials the surface concentration of hydroxyl radicals becomes high and OER (reaction 7 in Supporting Information) is promoted. Therefore, at the potential giving the signal current maximum, it is considered that the rates of both reaction are balanced. This is consistent with the similar background currents (about $30\,\mu A$) at the potential at which the signal current maxima with BDD-A, -B, and -C are observed. On the other hand, BDD-D and glassy carbon (GC) do not give

Phys. Status Solidi A 211, No. 12 (2014)

2715

apparent signals with injection of formic acid and the variation of the background current is much different from those with the other BDD electrodes. This indicates that the OER mechanism for the BDD-D is similar to a GC electrode and different from the other BDD electrodes, and that the sp^2-bonded carbon plays a major role in catalyzing the reaction. Possibly because the surface functionalities that can react with hydroxyl radicals catalyze the OER, the reaction of formic acid and hydroxyl radicals hardly occurred in BDD-D.

3.4 For ozone production The capability of the individual BDD electrodes for electrochemical ozone production (EOP) was investigated. The EOP mechanism is also initiated by the discharge of water and the hydroxyl radicals change the form toward ozone on the anode surface, as shown in Scheme S2, shown in Supporting Information. Figure 6 shows the transition curves of ozone concentration $[O_3]$ in pure water electrolyzed through an electrochemical flow cell with each BDD anode. The average $[O_3]$, and the current and cell voltage in the stable region between 30 and 90 s are summarized in Table 3, and the current efficiency, ε_{O_3}, and specific power consumption of the electrolytic cell, P, were calculated [9] and these are also summarized in Table 3.

The results for the BDD-A and BDD-B showed similar abilities for EOP as well as the other measurements presented above. All the measurements suggest the presence of sp^2-bonded carbon impurities in moderately BDD has little influence on the electrochemical properties. Heavily BDD, BDD-C, and BDD-D, exhibited high current efficiencies for EOP compared to moderately BDD. In particular, BDD-D showed a much higher concentration of ozone with high current efficiency.

From the EOP scheme, it is assumed that the density of active sites is an important factor because a high density of active sites leads to an increase in the frequency of encounters between adsorbed oxygen atoms and adsorbed O_2 (reaction 10 in Supporting Information (SI)). Accordingly, it is consistent that heavily BDD possessing a larger number of active sites has a high current efficiency. Additionally, sp^2-bonded carbon impurities in BDD-D might play a role not only as active sites but also as stronger adsorption sites. This can give longer adsorption time and longer adsorption of oxygen could promote the ozone formation (reaction 11 in SI). On the other hand, the BDD-D showed a poor capability for wastewater treatment, as noted above. Although both applications have in common the utilization of active oxygen species generated at the anode by application of a high potential in water, the properties required for both applications are not exactly the same. In the case of wastewater treatment, long lifetime of hydroxyl radicals is needed because the hydroxyl radical is a reactant for the combustion of organics. On the other hand, in the case of EOP, oxygen radicals, and oxygen that are formed thorough further oxidation of hydroxyl radical are reactants to form ozone. In terms of BDD-D, the sp^2-bonded species provide the sites for adsorbed oxygen radicals and the sites contribute to the ozone-formation reaction. On the other hand, glassy carbon electrodes to the ozonized water production measurement could not be endured because of its low durability against high voltage. Additionally, the ozone concentration of their electrolyzed water was very low compared to BDD electrodes (data not shown).

Consequently, the significant effects on the electrochemical properties were observed for heavily BDD but not for moderately BDD. In BDD-B and BDD-D, it is considered that the fraction of sp^2-bonded carbon might be very low and hence not enough to deform the bulk structure of diamond because prepared BDD have showed durability of diamond and typical morphology of polycrystalline diamond even for BDD-D. In fact, notable damages by anodic oxidation could not be observed in BDD-D with a scanning electron microscope (Fig. S2, SI). However, almost all grains consisting of BDD-D possess rough facets even before anodic oxidation although microstructure and morphology are similar to diamond. These indicate that drastic changes of the electrochemical properties of BDD-D by anodic treatment were caused by the changes in surface chemistry but not by changes in microstructure. Based on the experimental results, the surface of BDD-D possesses many more active sites, allowing adsorption for the species

Figure 6 The transition curves of the ozone concentration of electrolyzed water through an electrochemical flow cell with BDD anodes.

Table 3 Summary of results from electrochemical ozone-production measurements.

sample	ozone concentration (ppm)	current (A)	voltage (V)	current efficiency (%)	P (Wh g^{-1})
BDD-A	2.10	2.65	11.8	17.2	231
BDD-B	2.21	2.99	11.8	16.1	246
BDD-C	5.17	3.49	11.8	32.2	123
BDD-D	8.43	3.97	11.6	46.1	84.1

such as oxygen compared to the other BDD. Probably, the unusual adsorption properties compared to general BDD electrode are due to relaxation of the strain derived from both the doping atoms and the introduction of the sp^2-bonded species. It is quite likely that the rough facets of BDD-D are also caused by surface relaxation. Consequently, a large number of active sites like the edge plane of sp^2-bonded carbon material could be formed at the surface and BDD-D showed active electrochemical behaviors.

On the other hand, BDD-B showed no major difference in electrochemical properties compared to BDD-A despite with the presence of sp^2-bonded carbon impurities. In other words, there is no differences in adsorbing properties between BDD-A and BDD-B. Accordingly, it is assumed that there are not many adsorption active sites on the surface of BDD-B because of lower concentration of boron impurities. Alternatively, the adsorption active sites might not be electrochemically activated since the semiconducting BDD inhibit carrier transportation to such sites due to an energetic barrier like a Schottky junction. However, more variety of BDD samples and further structural analyses are required for verification of the above hypothesis. Our present studies are investigating the structure deformed by boron or sp^2-bonded carbon impurities in BDD with transmission electron microscopy (TEM).

4 Conclusion The physical and electrochemical properties of boron-doped polycrystalline diamond electrodes, prepared with four different boron doping levels and sp^2-bonded carbon impurities, were investigated. With respect to the difference in boron doping density, as expected, the heavily BDD electrodes exhibited narrower potential windows and a higher activity for redox reactions than the moderately BDD electrodes. In addition, an anodic treatment enhanced the differences between both types of BDD electrode. With respect to sp^2-bonded carbon impurities, the effects on the electrochemical properties were observed only with heavily BDD electrodes. The difference observed in heavily BDD is notable especially in the adsorption behavior.

The effects of sp^2-bonded carbon impurities in heavily BDD are probably due to an increase in adsorption active sites, which my be derived from surface relaxation of the strains induced by both impurities of boron and sp^2-bonded carbon atoms. However, further analyses for revealing atomic-scale structures of these films is needed to confirm the above hypothesis.

For electrochemical sensor applications, we conclude that, basically, heavily BDD is suitable because of the reliable response even against surface oxygenation and fast redox response. Although sometimes the wide potential window with low background current can be an important factor, BDD-A and B which had wider potential windows and also had a more sluggish response to the redox systems. Note that, of course, it depends on the sensing target. For wastewater treatment, moderately BDD and heavily BDD containing practically no sp^2-bonded carbon impurities are suitable as electrodes. Furthermore, because of the high electrochemical durability and high electrode activity, it is considered that heavily BDD containing sp^2-bonded carbon impurities possesses the potential for direct electrolysis applications, such as ozonized water production.

From a practical application perspective, this approach, whereby boron doping and the incorporation of sp^2-bonded carbon impurities are utilized, provides a guideline for designing diamond electrodes.

References

[1] M. C. Granger, J. S. Xu, J. W. Strojek, and G. M. Swain, Anal. Chim. Acta **397**(1–3), 145–161 (1999).
[2] R. G. Compton, J. S. Foord, and F. Marken, Electroanalysis **15**(17), 1349–1363 (2003).
[3] T. N. Rao, I. Yagi, T. Miwa, D. A. Tryk, and A. Fujishima, Anal. Chem. **71**(13), 2506–2511 (1999).
[4] J. Iniesta, P. A. Michaud, M. Panizza, G. Cerisola, A. Aldaz, and C. Comninellis, Electrochim. Acta **46**(23), 3573–3578 (2001).
[5] Q. Y. Chen, M. C. Granger, T. E. Lister, and G. M. Swain, J. Electrochem. Soc. **144**(11), 3806–3812 (1997).
[6] Q. Y. Chen and G. M. Swain, Langmuir **14**(24), 7017–7026 (1998).
[7] G. M. Swain, Adv. Mater. **6**(5), 388–392 (1994).
[8] B. Marselli, J. Garcia-Gomez, P. A. Michaud, M. A. Rodrigo, and C. Comninellis, J. Electrochem. Soc. **150**(3), D79–D83 (2003).
[9] K. Arihara, C. Terashima, and A. Fujishima, J. Electrochem. Soc. **154**(4), E71–E75 (2007).
[10] C. Levy-Clement, F. Zenia, N. A. Ndao, and A. Deneuville, New Diam. Front. Carbon Technol. **9**(3), 189–206 (1999).
[11] M. N. Latto, G. Pastor-Moreno, and D. J. Riley, Electroanalysis **16**(6), 434–441 (2004).
[12] D. A. Tryk, K. Tsunozaki, T. N. Rao, and A. Fujishima, Diam. Relat. Mater. **10**(9–10), 1804–1809 (2001).
[13] J. A. Bennett, J. A. Wang, Y. Show, and G. M. Swain, J. Electrochem. Soc. **151**(9), E306–E313 (2004).
[14] S. Alehashem, F. Chambers, J. W. Strojek, G. M. Swain, and R. Ramesham, Anal. Chem. **67**(17), 2812–2821 (1995).
[15] E. Bustarret, P. Achatz, B. Sacépé, C. Chapelier, C. Marcenat, L. Ortéga, and T. Klein, Philos. Trans. R. Soc. A **366**(1863), 267–279 (2008).
[16] M. I. Landstrass and K. V. Ravi, Appl. Phys. Lett. **55**(10), 975–977 (1989).
[17] F. Maier, M. Riedel, B. Mantel, J. Ristein, and L. Ley, Phys. Rev. Lett. **85**(16), 3472–3475 (2000).
[18] J. S. Xu, Q. Y. Chen, and G. M. Swain, Anal. Chem. **70**(15), 3146–3154 (1998).
[19] J. Robertson, 1997 (unpublished).
[20] U. Fano, Phys. Rev. **124**(6), 1866 (1961).
[21] F. Pruvost and A. Deneuville, Diam. Relat. Mater. **10**(3–7), 531–535 (2001).
[22] P. Gonon, E. Gheeraert, A. Deneuville, F. Fontaine, L. Abello, and G. Lucazeau, J. Appl. Phys. **78**(12), 7059–7062 (1995).
[23] N. Wada and S. A. Solin, Physica B + C **105**(1–3), 353–356 (1981).
[24] A. J. Bard and L. R. Faulkner, Electrochemical Methods: Fundamentals and Applications. second ed. (John Wiley, New York, Chichester, 2001).

Phys. Status Solidi A 211, No. 12 (2014)

Original
Paper

2717

[25] T. Watanabe, T. K. Shimizu, Y. Tateyama, Y. Kim, M. Kawai, and Y. Einaga, Diam. Relat. Mater. **19**(7–9), 772–777 (2010).

[26] A. Suzuki, T. A. Ivandini, K. Yoshimi, A. Fujishima, G. Oyama, T. Nakazato, N. Hattori, S. Kitazawa, and Y. Einaga, Anal. Chem. **79**(22), 8608–8615 (2007).

[27] D. A. Tryk, H. Tachibana, H. Inoue, and A. Fujishima, Diam. Relat. Mater. **16**(4–7), 881–887 (2007).

[28] C. Comninellis, Electrochim. Acta **39**(11–12), 1857–1862 (1994).

[29] H. B. Yu, C. J. Ma, X. Quan, S. Chen, and H. M. Zhao, Environ. Sci. Technol. **43**(6), 1935–1939 (2009).

Supporting Information

Additional supporting information may be found in the online version of this article at the publisher's website.